Title

Halide anion discrimination by a tripodal hydroxylamine ligand in gas and condensed phases

Journal

Physical Chemistry Chemical Physics, 21(36)

ISSN

0956-5000

Authors

Cheisson, Thibault

Jian, Jiwen

Su, Jing

et al.

Publication Date

2019-09-18

DOI

10.1039/c9cp03764k

Peer reviewed

ARTICLE

Halide Anion Discrimination by a Tripodal Hydroxylamine Ligand in Gas and Condensed Phases

Received 00th January 20xx,
Accepted 00th January 20xx

DOI: 10.1039/x0xx00000x

Thibault Cheisson,[†,a] Jiwen Jian,[†,b,d] Jing Su,[†,c] Teresa M. Eaton,[b,e] Michael R. Gau,[a] Patrick J. Carroll,[a] Enrique R. Batista,*[,c] Ping Yang,*[,c] John K. Gibson,*[,b] and Eric J. Schelter*[,a]

Electrospray ionization of solutions containing a tripodal hydroxylamine ligand, H_3TriNOx ([((2-^{t}BuNOH)$C_6H_4CH_2)_3$N]) denoted as L, and a hydrogen halide HX: HCl, HBr and/or HI, yielded gas-phase anion complexes $[L(X)]^-$ and $[L(HX_2)]^-$. Collision induced dissociation (CID) of mixed-halide complexes, $[L(HX_aX_b)]^-$, indicated highest affinity for I^- and lowest for Cl^-. Structures and energetics computed by density functional theory are in accord with the CID results, and indicate that the gas-phase binding preference is a manifestation of differing stabilities of the HX molecules. A high halide affinity of $[L(H)]^+$ in solution was also demonstrated, though with a highest preference for Cl^- and lowest for I^-, the opposite observation of, but not in conflict with, what is observed in gas phase. The results suggest a connection between gas- and condensed-phase chemistry and computational approaches, and shed light on the aggregation and anion recognition properties of hydroxylamine receptors.

Introduction

Halide anions are prevalent in essentially all aspects of chemistry, with their use, transport, speciation, and reactivity being critical to processes ranging from those in living organisms[1] to nuclear technologies. In the latter case, uranium is enriched through its volatile hexafluoride salt,[2] plutonium legacy-waste contains high chloride concentrations,[3-4] while iodine-129 is an abundant long-lived (half-life = 1.57×10^7 y) fission product generated in nuclear reactors.[5] As a consequence, halides represent a substantial fraction of low-, intermediate-, and high-level wastes.[6-7] Vitrification has been proposed for long-term immobilization and sequestration of radionuclides.[8-10] However, incorporation of a large concentration of halide anions is detrimental to the quality and sustainability of the formed glass such that these anions must be separated prior to vitrification.[6-7, 11-12] Typical methodologies encompass precipitation, reduction to the volatile elemental gas, or anion exchange.[6] On the other hand, halide binding and recognition have been long-standing[13-15] subjects of interest in supramolecular chemistry.[16-23] Although other strategies have been proposed,[22, 24] the hydrogen bond motif has been ubiquitous in these systems. In that context, functional groups such as (thio)urea, amide, pyrrole, or imidazole have attracted considerable attention due to their donor/acceptor properties and geometrical features.[15, 22-23]

Given our interest in hydroxylamine ligands (R^1R^2NOH),[25-31] and recognizing their potential for anion binding by means of vicinal H-bond acceptors associated with mildly acidic protons, we initiated studies on the propensity of a tripodal receptor (H_3TriNOx) for anion capture (Scheme 1). As hydroxylamine moities have not been examined in this context previously, it was of interest to interrogate their interactions with halides under a range of conditions, including condensed and gas phases, to determine fundamental thermodynamic trends.

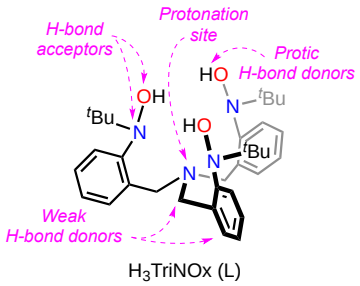

Scheme 1. Structure and characteristics of H_3TriNOx (L) and the halide anions considered in this work. Ionic radii according to Shannon;[32] electronegativities ($\overline{\chi}$) according to Rahm.[33]

Gas-phase ion chemistry is a versatile technique for obtaining fundamental insights for relatively simple systems absent perturbations encountered in condensed phases.[34-36] A particularly functional approach is solution electrospray

[a.] P. Roy and Diana T. Vagelos Laboratories, Department of Chemistry, University of Pennsylvania, 231 S 34th St., Philadelphia, PA 19104 (USA) E-mail: schelter@sas.upenn.edu
[b.] Chemical Sciences Division, Lawrence Berkeley National Laboratory, Berkeley, CA 94720 (USA) E-mail: jkgibson@lbl.gov
[c.] Theoretical Division, Los Alamos National Laboratory, Los Alamos, NM 87545 (USA), E-mails: erb@lanl.gov; pyang@lbl.gov
[d.] Present address: Hangzhou Institute of Advanced Studies, Zhejiang Normal University, 1108 Gengwen Road, Hangzhou, Zhejiang, China, 311231.
[e.] Present address: Embry-Riddle Aeronautical University, Department of Natural Sciences, 3700 Willow Creek Road, Prescott, AZ 86301 (USA)
† These authors contributed equally.
Electronic Supplementary Information (ESI) available: Gas- and condensed-phase methods and characterization, computational and crystallographic details. See DOI: 10.1039/x0xx00000x

ionization mass spectrometry (ESI-MS) which, coupled to a quadrupole ion trap mass analyser (QIT/MS), can be used to study ion fragmentation.[37] Various types of gas-phase complexes and clusters with generic anion-binding interactions of the type $[E–H^{\delta+}\cdots X^-]$ (E = N, C, O; X = F, Cl, Br, I) have previously been studied.[38-45]

In the present work, condensed phase experiments revealed the intrinsic halide (X^-) affinity of protonated H_3TriNOx, $[L(H)]^+$, to efficiently yield crystalline compounds with the formulae L(HX). Experimental and density functional theory (DFT) studies of gas-phase anionic $[L(X)]^-$ and $[L(HX_2)]^-$ complexes were performed to elucidate the underlying basis for anion recognition by L. Altogether the combined gas and condensed phase studies of L(HX) complexes reveal hydroxylamine as an interesting motif for selective anion binding.

Results and Discussion

ESI Mass Spectrometry.

During an ESI-MS study of binding affinity of L for actinides and rare-earth elements,[46] our attention was drawn by abundant anion complexes with compositions $[L(HX_2)]^-$. Although ESI-MS does not necessarily explicitly reveal solution species, the gas-phase species may indirectly reflect solution affinities. The observed $[L(HX_2)]^-$ ions were independently and rationally formed from solutions of L and acids $HX_{(aq)}$ with X = Cl, Br, I. Formation of these di-halide adducts motivated the preparation of gas-phase species such as $[L(HX_aX_b)]^-$ with two halides, X_a and X_b. Indeed, collision induced dissociation (CID) of such mixed halide complexes can reveal preferred elimination pathways, that in turn reflect structures and energetics that can be directly assessed by computations. The utility of ESI-MS and CID for assessing structures and bonding of halide complexes has been described.[47-48]

For X_a= Cl and X_b = Br (Figure 1a), the dominant observed gas-phase complexes from ESI were $[L(Cl)]^-$, $[L(Br)]^-$, $[L(HClBr)]^-$, $[L(HCl_2)]^-$, and $[L(HBr_2)]^-$. This nomenclature is not intended to suggest structural or bonding insights, but rather only net compositions. The most abundant complexes in Figure 1a, $[L(HClBr)]^-$ and $[L(HBr_2)]^-$, contain one or two Br, possibly suggesting a higher affinity of L for Br^- versus Cl^-. The gas-phase species $[L(HBr_2)]^-$ may also be present in solution, either as a monomer, or in oligomers that fragment during ESI. This possibility was assessed by the condensed phase experiments discussed below. Although small abundances of $[L(Cl)]^-$ and $[L(Br)]^-$ were apparent, ESI resulted in preferential formation of the complexes with two halide anions.

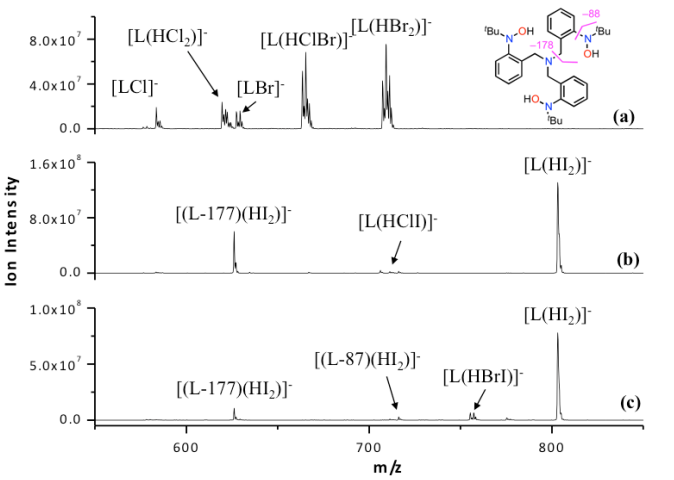

Figure 1. Negative-ion mode ESI mass spectra of solutions of L and equal concentrations in ethanol of two halide acids, HX_a and HX_b: (a) HCl and HBr; (b) HCl and HI; (c) HBr and HI. The $L:HX_a:HX_b$ ratios are all 1:5:5. The ligand fragmentation patterns are indicated in the structural inset.

The ESI results for solutions containing I^- and either Cl^- or Br^- (Figure 1b–c), suggest a higher affinity of L for I^- as compared with both Cl^- and Br^-, at least under these particular ion production conditions (*vide infra*). It should also be emphasized that ESI yields do not necessarily reveal solution affinity. For example, ESI may be more sensitive to larger halides such as iodide due to its less effective solvation. It is nonetheless notable that the overwhelmingly dominant ESI products contain only iodide — i.e. $[L(HI_2)]^-$ and $[(L–177)(HI_2)]^-$ — with only minor yields of $[L(HClI)]^-$ and $[L(HBrI)]^-$. A distinctive result is the appearance of substantial $[(L–177)(HI_2)]^-$, where (L–177) indicates an H_3TriNOx that has lost a fragment having a mass of 177 Da. This same fragmentation is observed in CID of protonated $[L(H)]^+$ (Figure S1) and corresponds to C–N bond cleavage and elimination of one of the three H_3TriNOx "arms" with concomitant back-transfer of an H atom, as indicated by the purple line in Figure 1. Although the origins of the characteristic L–177 species are unknown, it suggests a distinctive interaction of I^- with L. It is re-emphasized that such gas-phase species do not necessarily reflect solution speciation. The ESI results demonstrate the formation of gas-phase $[L(HX_aX_b)]^-$ anions and suggest the preferential association of heavier halides. In order to interrogate this trend we turned to CID experiments on these ions.

Collision Induced Dissociation.

CID performed on the $[L(HX_aX_b)]^-$ anions are presented in Figure 2 and show exclusively one CID fragmentation pathway for each of the studied complexes, as given by reactions (1a)–(3a):

$[L(HClBr)]^- \rightarrow [L(Br)]^- + HCl$ (1a)

$[L(HClI)]^- \rightarrow [L(I)]^- + HCl$ (2a)

$[L(HBrI)]^- \rightarrow [L(I)]^- + HBr$ (3a)

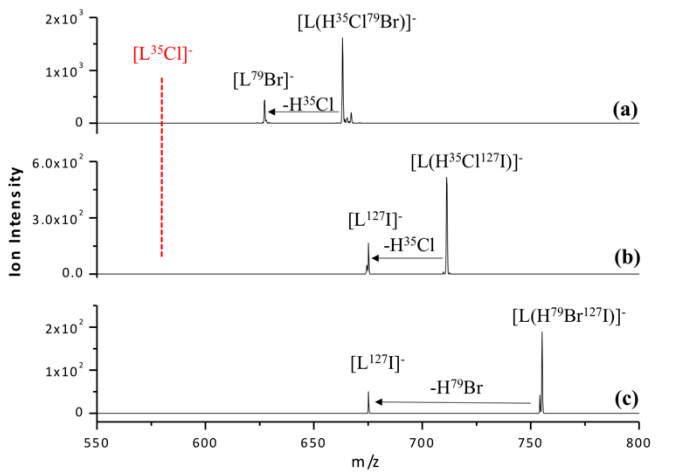

Figure 2. CID mass spectra of $[L(HX_aX_b)]^-$ anions (X = Cl^-, Br^-, I^-). (a) $[L(HClBr)]^-$ / CID amplitude = 0.30 V; (b) $[L(HCl)]^-$ / CID = 0.30 V; (c) $[L(HBrI)]^-$ / CID = 0.35 V.

Alternative CID pathways, namely reactions (1b)–(3b), described as the loss of $HBr_{(g)}$ as an alternative to reaction (1a) and loss of $HI_{(g)}$ as an alternative to reactions (2a) and (3a), were not observed.

Lighter CID anion products such as bare Cl^-, Br^-, and I^- would not have been detected due to m/z detection limits. In Figures 2a and 2b, the m/z of unobserved $[L(^{35}Cl)]^-$ is indicated in red. Endothermic CID process is governed by two attributes: (i) lower-energy processes are generally favored; and (ii) kinetic barriers may instead favor higher-energy processes. Elimination of neutral HX_a from $[L(HX_aX_b)]^-$ presumably proceeds by low-barrier association of H^+ with X_a^- to produce $[L(X_b)]^-$. This hypothesis is supported by computational results which indicate that observed CID pathways are energetically favored and the kinetic barrier is not a determining factor.

In addition to relative stabilities of the parent and CID-generated anion complexes, the overall energetics of the observed CID processes, generic reaction (4), incorporate the formation energy of produced neutral HX_b, which is assessed from reaction (5):

$[L(HX_aX_b)]^- \rightarrow [L(X_b)]^- + HX_a$ (4)

$H + X_a \rightarrow HX_a$ (5)

The energy (kcal mol^{-1}) for reaction (5) is −103 for HCl, −87 for HBr, and −71 for HI.[49-50] Neutral HX formation energies from atomic H and X thus favor CID fragmentation to yield HCl over HBr over HI, in 16 kcal mol^{-1} increments. Formation energies of HX from molecular H_2 and X_2 are -92, -52, and -5 kJ mol^{-1} for HCl, HBr and HI, respectively; the same stability trend is obtained though with larger incremental energy differences. Although the CID results given by reactions (1a), (2a), and (3a) would appear to suggest a higher affinity of L for I^- over Br^- over Cl^-, the observed pathways could be partially, or perhaps mostly, a manifestation of the higher stability of gas-phase HCl over HBr over HI. An alternative conceptualization of reaction (4) is from the perspective of Cooks' kinetic method,[51] whereby halide X_a^- or X_b^- with the higher proton affinity (PA) preferentially retains the proton. Because the order of PAs is Cl^- (333 kcal mol^{-1}) > Br^- (323) > I^- (314),[49] this alternative assessment presents the same conclusion as reaction (5), though the incremental difference in PAs is ca. 10 rather than 16 kcal mol^{-1}. As discussed below, the observed fragmentation pathways may also be partly a manifestation of structures that favor a particular proton-halide recombination.

In view of the neutral HX energetics, the CID results do not necessarily reveal an intrinsically higher gas-phase affinity of H_3TriNOx for I^- over Br^- over Cl^-. The computational results below for reactions (1)–(3) yield an assessment of the energetics, as well as possible influence of anion complex structures on favored fragmentation pathways.

Computations: Structures Optimization.

To gain insights into the apparently higher affinity of L for heavier halides, we turned to DFT (B3LYP-D3BJ/6-311G**) calculations. Different possible conformers of $[L(HX_2)]^-$, the mixed halide complexes $[L(HX_aX_b)]^-$, and $[L(X)]^-$ (X = Cl, Br, I) were sampled and optimized (Tables S1–S3).

The lowest energy conformer for all three $[L(HX_2)]^-$ complexes (isomers $\mathbf{1_X}$ in Figure 3A and Table S1) presents a "Janus head" conformation. Namely, a halide atom is coordinated by the protonated ammonium and a hydroxylamine moiety on one side of the receptor, while the second halide is coordinated by two hydroxylamine groups on the opposite side of the ligand.

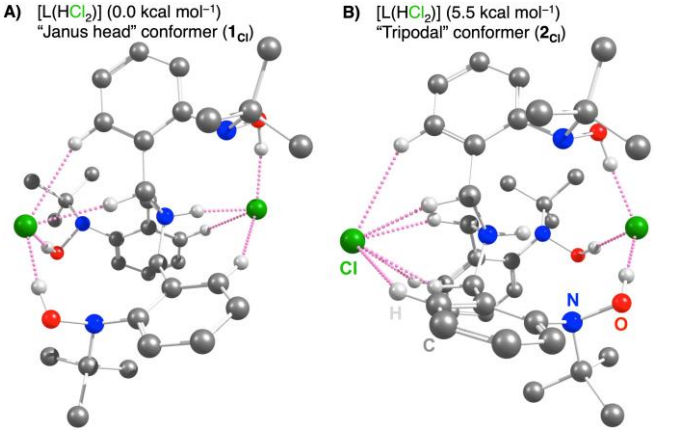

Figure 3. DFT-optimized conformers of $[L(HCl_2)]$: "Janus head" form (A) and "Tripodal" form (B). Most significant H-bonding interactions (d < 3 Å) are displayed as pink dotted lines; other hydrogen atoms were omitted for clarity.

A second set of conformers (isomers $\mathbf{2_X}$ in Figure 3B and Table S1), higher in energy (+5.4 to 5.6 kcal mol^{-1}), shows a C_3-symmetric "tripodal" conformation where the three hydroxylamine moieties interact with a first halide. On the other side, the second halide is stabilized by weak but abundant CH---X interactions. Such short contacts have been observed, experimentally and computationally, to contribute significantly or exclusively to halide binding and recognition.[23, 52-56] Notably the lower energy conformers $\mathbf{1_X}$ and $\mathbf{2_X}$ for gas-phase DFT-optimized $[L(HX_2)]^-$ units were reminiscent to the geometries revealed by solid-state crystallography as discussed below.

For the mixed halide compounds $[L(HX_aX_b)]^-$, the "Janus head" conformers are also energetically favored over the "tripodal" forms (Table S3). In this case, the site selectivity can be interrogated by DFT, the results are depicted in Table S3 and in Figure 4 for the specific case of $[L(HClBr)]^-$. In the most stable isomers (**1a**), the heavier halide anions (X_b) are observed to

interact with the ammonium and one hydroxylamine arm, while the lighter halide (X_a) forms H-bonds with the remaining two hydroxylamine groups in the other side of the receptor. However, swapping the two halides in **1a** to yield isomer **1b** requires only +0.6–1.3 kcal mol^{-1}, with the lowest swapping energy for Cl^-/Br^- and the highest for Cl^-/I^- (Table S2).

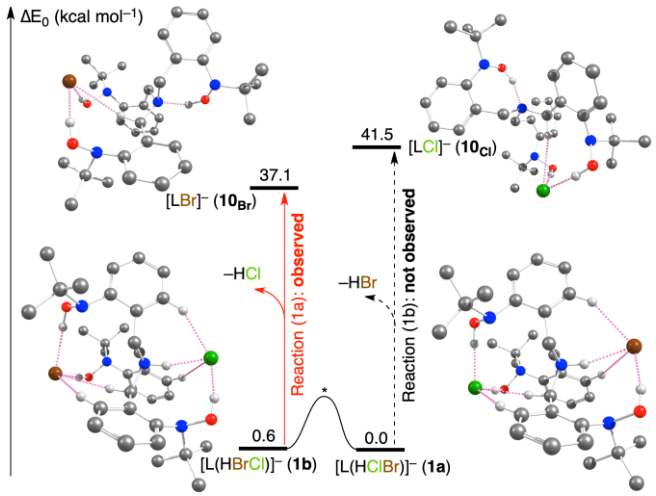

Figure 4. Calculated DFT profiles for the CID process (1), DFT-optimized of the different structures are depicted, the most significant H-bonding interactions are displayed as pink dotted lines. * Interconversion barriers and pathways were not computed.

In order to assess the stability of the products $[L(X)]^-$ in reactions (1)–(3), different $[L(X)]^-$ were also optimized (Figure 4 and Table S3). Again, isomers $\mathbf{11_X}$ possessing tripodal geometries are located higher in energy (0.5 to 5.0 kcal mol^{-1}) than isomers $\mathbf{10_X}$ presenting the Janus head conformation. As depicted in Figure 4, the conformers $\mathbf{10_X}$ are binding the remaining halide with 2 hydroxylamine arms and some CH---X contacts, while the third NOH group interacts with the, now neutral, bridgehead nitrogen atom. Notably, the lowest energy conformer for $[L(I)]^-$ is $\mathbf{13_I}$, found slightly below $\mathbf{10_I}$ (1.4 kcal mol^{-1}). In this conformer, L adopts a tripodal conformation with an internal, intramolecular, H-bonding network—typical of the free ligand[25]—while the iodide anion is stabilized by multiple CH---I interactions with the benzylic protons (Table S3). The increasing relative stability of $\mathbf{13_X}$ versus $\mathbf{10_X}$ for $[L(X)]^-$ isomers from X = Cl to Br to I seems correlated with the decreasing X---H(O/C) interactions as observed in the literature.[57-58]

With these sets of optimized conformers in hand, the different CID pathways can now be modelled as discussed below.

Computed CID Energetics.

According to the generic reaction (4), dissociations and reverse associations ($[L(X_a)]^- + HX_b \rightarrow [L(HX_aX_b)]^-$) were evaluated for $X_a = X_b$ and $X_a \neq X_b$. All the association reactions are exothermic, by −34.6 to −45.2 kcal mol^{-1} (Table S4) in accord with the low yields of $[L(X)]^-$ anions over $[L(HX_2)]^-$ observed by ESI (Figure 1). For a given $[L(X_a)]^-$, preferential affinity for heavier halides was consistently observed. For example in the reaction $[L(I)]^- + HX_b \rightarrow [L(HIX_b)]^-$, the binding energy of $[L(I)]^-$ to HX_b increases from 34.6 to 37.9 to 40.6 kcal mol^{-1} as X_b becomes heavier from Cl to Br to I. The increase in binding energy from Cl to Br to I seems to be in accord with the dominance of the heavier halide complexes from ESI (Figure 1), but inference of solution speciation from these spectra must be qualified, as discussed below.

The reverse of the above complexation reactions for $X_a \neq X_b$ corresponds to CID fragmentation of the mixed halides $[L(HX_aX_b)]^-$. The calculated fragmentation reaction energies in Table 1 and S5 show that for a given $[L(HX_aX_b)]^-$, loss of the lighter HX_a requires less energy by 4.4–10.6 kcal mol^{-1}. This is illustrated in Figure 4 for the specific case of $L(HClBr)]^-$ where loss of $HCl_{(g)}$ (reaction 1a) over $HBr_{(g)}$ (reaction 1b) is favored by 4.4 kcal mol^{-1} in accord with the CID results in Figure 2.

Besides reproducing accurately the energetics for the net equations (1a), (2a), and (3a); these results also indicate that kinetic barriers do not play a significant role in controlling the final products. From the structures of isomers **1a** and **1b** of $[L(HClBr)]^-$ (Figure 4), it is evident that loss of HBr, which is computed at higher energy than loss of HCl, can only readily proceed from the lowest energy conformer **1a** via direct recombination of the ammonium proton and the proximate bromide anion. The lower-energy elimination of HCl is not as directly accessible from this structure. In summary, the calculation results indicate that for $[L(HX_aX_b)]^-$ loss of HX_a is favored thermodynamically but not kinetically for X_a lighter than X_b.

Table 1. Dissociation energies for $[L(HX_aX_b)]^-$ (kcal mol^{-1}). Bolded values represent the lowest energy pathway.

Halides	DFT[a]		"Intrinsic" [b]	
$[L(HX_aX_b)]^- \rightarrow$	$[L(X_a)]^-$ + HX_b	**$[L(X_b)]^-$ + HX_a**	**$[L(X_a)]^-$ + H + X_b**	$[L(X_b)]^-$ + H + X_a
X_a = Cl, X_b = Br	41.5	**37.1**	**118**	130
X_a = Cl, X_b = I	45.2	**34.6**	**104**	129
X_a = Br, X_b = I	44.0	**37.9**	**103**	115

[a] DFT-calculated energies for the CID pathways. [b] Hypothetical dissociation equation using tabulated energies for HX.[49-50]

Nature of the Experimental CID.

As indicated, the computed fragmentation energies (Figure 4 and Table 1) demonstrate that fragmentation of $[L(HX_aX_b)]^-$ to $[L(X_b)]^-$ and HX_a, where X_a is the lighter halide, is favored by 4.4–10.6 kcal mol^{-1}. Notably, these energy differences are significantly less than the 16–32 kcal mol^{-1} differences for reaction (5) that favor formation of the lighter HX_a from the association of H and X_a, as discussed above.[49-50] Accordingly, the differences in energetics for the dissociation reactions in Table 1 do not appear to reflect an inherently greater stability of $[L(X_a)]^-$ versus $[L(X_b)]^-$, as for example $[L(I)]^-$ versus $[L(Cl)]^-$. Instead, the computed energetics evidently reflects the trend in increasing stability of the produced HX: HI < HBr < HCl. If adjustment is made for the relative H + X_a association energies, reaction (5), the derived fragmentation energies in Table 1 for reaction (6) actually suggest that the intrinsic stabilities increase in the order $[L(I)]^- < [L(Br)]^- < [L(Cl)]^-$, which is the opposite of what might be casually inferred from the CID results in Figure 2.

$$[L(HX_aX_b)]^- \rightarrow [LX_b]^- + H + X_a \qquad (6)$$

The CID results appear to be a manifestation of the higher stabilities of the produced HX_a rather than the intrinsic stabilities of the $[LX_b]^-$.

Synthesis and Structural Characterization.

In order to provide a condensed-phase basis for comparison with the gas-phase results presented above, we targeted the synthesis of the series of L(HX) (X = F, Cl, Br, and I) compounds. Addition of an excess of the $HX_{(aq)}$ acid to an ethanol solution of L followed by precipitation in water afforded the salts L(HX) in moderate to good yields (Scheme 2).

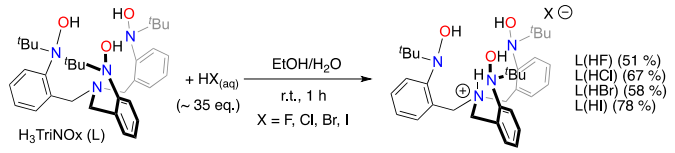

Scheme 2. Synthesis of L(HX) (X = F, Cl, Br, I)..

The isolated salts L(HX) revealed identical ESI products as the results presented in Figure 1 (Figures S6–S7). Compounds L(HX) were characterized by ^{1}H and ^{13}C{^{1}H} NMR, infrared (IR) spectroscopy, solution electrochemistry, and elemental analysis, confirming protonation of L to yield the different ammonium salts. Going from L(HCl) to L(HI), electrochemical measurement revealed a shift to lower potential for the oxidation of the hydroxylamine moieties to their nitroxide (Figure S26). IR spectra of L(HX) revealed a gradual shift to lower frequencies for the NOH stretches going from X = I to F (Figure S27). This trend and the overall spectra were well-reproduced in the predicted IR spectra of DFT-optimized isomers $\mathbf{1_X}$ of $[L(HX_2)]^-$ (Figure S28). This suggests large structural similarities between the lowest-energy calculated conformers of $[L(HX_2)]^-$ and solid-state L(HX) as confirmed by solid-state crystallography (*vide infra*). ^{1}H NMR studies in CD_2Cl_2 demonstrated C_{3v} symmetric species on the NMR timescale at 300 K. Variable temperature NMR studies revealed broadening of most resonances caused by the crystallization of the salts at lower temperature (Figure S29). Particularly interesting was comparison of the ^{1}H NMR spectra of L(HX), which demonstrates a gradual increase in the shielding of the hydroxylamine protons from L(HF) to L(HI), in agreement with the decreasing electronegativity of the respective halides from F^- to I^- (Figure S30).[59] Taken together, the spectroscopic data were in accord with the protonation of L at the bridgehead nitrogen atom and association of the halide anions through H-bond interactions with the hydroxylamine moieties. The chloride, bromide, and iodide salts were recrystallized in ethanol and provided suitable crystals for X-ray diffraction (XRD) studies. L(HCl)·EtOH and L(HBr)·EtOH were isostructural and crystallized as a 1D-H-bonded coordination polymer (Figure 4A for L(HCl)·EtOH and S37 for L(HBr)·EtOH). In these structures, the $[L(H)]^+$ cations lack any C_3 symmetry and present a "Janus head" conformation noted in the gas-phase DFT-optimized structures: on one side of $[L(H)]^+$, a hydroxylamine group and the ammonium proton interact with a halide anion; on the other side, an ethanol molecule and the remaining two hydroxylamine moieties are involved in a H-bonding network with the anion. The repetition of this motif generates the observed supramolecular polymer (Figure 4A). The solid-state structure of L(HI)·½EtOH was slightly different and consisted of two independent $[L(H)]^+$ units. The first one presents a similar "Janus head" arrangement as observed in L(HCl)·EtOH and L(HBr)·EtOH, while the second $[L(H)]^+$ acts as a discrete anion receptor with the "tripodal" configuration (Figure 4B). In this case, the supramolecular chain was permitted by multiple CH---I(1) interactions from the benzylic protons of $[L(H)]^+$ (H(1b'), H(12b'), H(23b') on Figure 4B). Importantly, this motif of interaction was only noticed for L(HI) and is reminiscent to the geometry of the most stable isomer of $[L(I)]^-$ ($\mathbf{13_I}$) obtained during the gas-phase DFT optimizations.

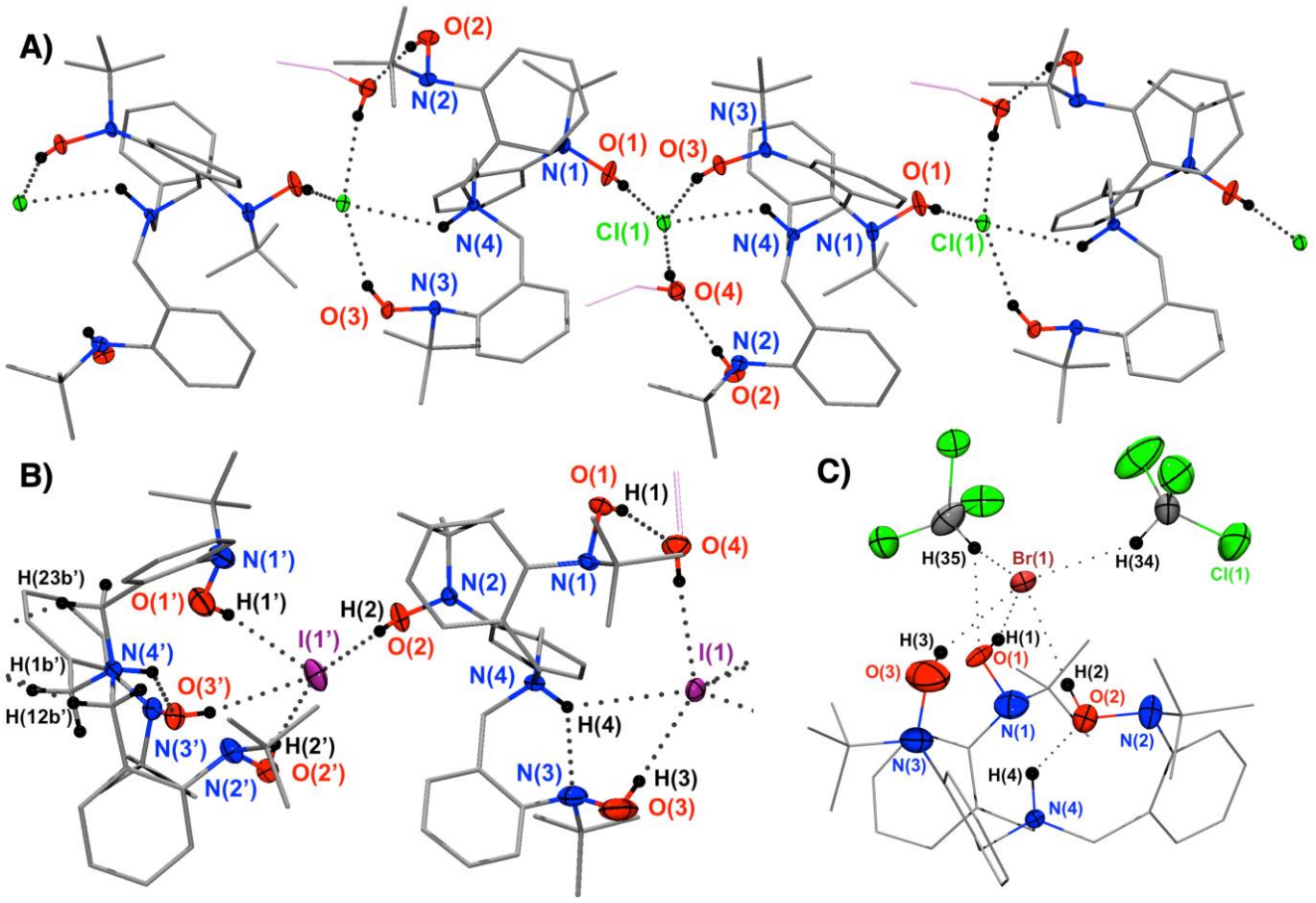

Figure 4. Solid-state structures of different salts; heteroatoms are depicted by their thermal ellipsoids, relevant hydrogen atoms are depicted in black, ethanol molecules in light pink. A) H-bonded polymer of L(HCl)·EtOH along the *a* axis. B) Asymmetric unit of L(HI)·½EtOH. C) Asymmetric unit of L(HBr)·2($CHCl_3$).

In the previous solid-state structures, an ethanol molecule was present and directly participated in the H-bond network, raising the question if its presence influences the crystal packing of L(HX). Compounds L(HCl) and L(HBr), recrystallized from benzene resulted in displacement of the ethanol molecule while preserving the 1D-H-bonded polymer, revealing that ethanol was not requisite for the observed crystal arrangement (Figure 5 and S38).

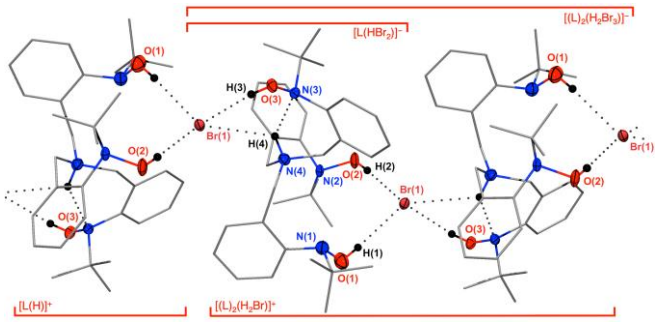

Figure 5. Solid-state structure of polymeric L(HBr) along the *b* axis as determined by X-ray crystallography. The proposed structures associated with the main ESI species (positive and negative mode) are depicted in red.

Despite multiple attempts, crystals of L(HF) suitable for XRD characterization were not obtained. In total, L(HX) are easily synthesized and form, in the solid-state, H-bonded polymers that reveal geometries closely related to the DFT-optimized structures.

Solution Speciation.

Although adducts L(HX) were characterized by NMR spectroscopy and crystallized as supramolecular polymers, we were interested in studying more in depth their solution-state speciation to relate with the ESI results. The existence of a soluble, extended polymeric structure is unlikely. When in solution, compounds L(HX) are expected to be present as monomer or small oligomer prior to their crystallization as an extended structure. Chlorinated solvents such as chloroform and dichloromethane were observed to efficiently solubilize (for extended periods of time) L(HCl), L(HBr), and L(HI). ^{1}H DOSY NMR studies performed on CD_2Cl_2 solutions of L and L(HBr) revealed similar diffusion coefficients suggesting similar hydrodynamic radii in solution. More importantly, cooling a solution of L(HBr) in $CHCl_3$ to −20 °C for a week resulted in the formation of single crystals suitable for X-ray diffraction studies (Figure 4C). The corresponding solid-state structure demonstrated a nearly C_3-symmetric $[L(H)]^+$ receptor binding to the bromide anion through the hydroxylamine moieties. Two chloroform molecules now supplement the coordination sphere of the bromide anion. From these observations, we propose that chloroform or dichloromethane solutions of L(HX) consist

of monomeric [L(HX)]·n(solv) (n ~ 2–3) with $[L(H)]^+$ in the "tripodal" form.

Halide Binding in Solution.

Having a clearer picture of the speciation of L(HX) in solution, we were interested in assessing the ability to bind a supplementary halide as suggested by the solid-state polymeric structures and the gas-phase experiments. Addition of $[N^nBu_4]X$ to a solution of the respective L(HX) salts (X = Cl, Br, I; L(HF) was not sufficiently soluble) resulted in important modifications in the resulting ^1H NMR spectra. In particular, NOH moieties and one aromatic proton experienced large deshielding (Figures S31–S36). Job's plots were in accord with a 1:1 binding model but the limited applicability of this method prompted us to evaluate alternative models.[60] The binding isotherms resulting from ^1H NMR titrations at 298 K were fitted to several stoichiometries, but were consistently in best agreement with a 1:1 model.[61] This was attributed to the formation of di-halide adducts $[L(HX_2)]N^nBu_4$ (Scheme 3). The binding constants K_X increased from 245 M^{-1} for I^- to 872 M^{-1} for Cl (Scheme 3) as observed in related systems.[55] Besides repeated attempts, single crystals of $[L(HX_2)]N^nBu_4$ could not be grown but it is proposed that these species adopt a "Janus head" conformation and to resemble isomers $\mathbf{1_X}$ of $[L(HX_2)]^-$ obtained by DFT methods (Table S1).

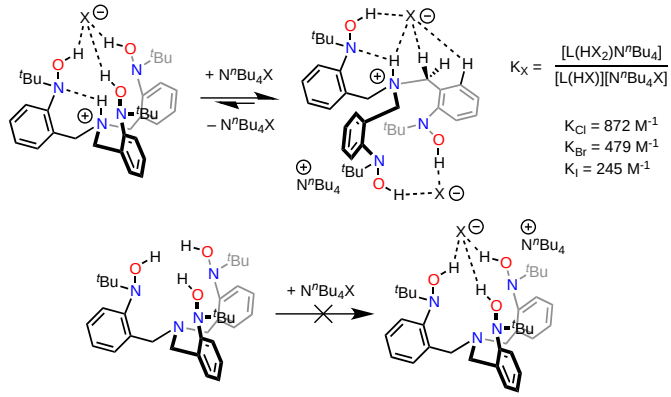

Scheme 3. Halide binding equilibria for L(HX), and free L.

To further confirm the stoichiometry of the binding model, we performed ^1H DOSY NMR studies which demonstrated a similar diffusion coefficient for L(HBr) and $[L(HBr_2)]N^nBu_4$, this suggests that, at the NMR timescale, no larger oligomer is formed, which allows us to further rule out a potential 2:1 binding model. Interestingly, titration experiments between L and $[N^nBu_4]X$ did not reveal any noticeable binding (Scheme 3).

Although there is about a 4-fold difference between K_{Cl} and K_I (which is small compared to other systems),[16, 62] this only corresponds to an energy difference, $\Delta\Delta G = RT\ln[K_{Cl}/K_I]$, of ~0.8 kcal mol^{-1}, which is small relative to differences in gas-phase energetics discussed above. These binding equilibria were also evaluated by DFT methods that are generally consistent with the experimental trend (Table S8). Overall, the titration results clearly demonstrate that L(HX) has a strong affinity for binding a second halide, as was also determined by the gas-phase experimental and theoretical results. This affinity contrasts with that of neutral L, suggesting that protonation pre-organizes a secondary anion receptor.

Gas Phase Oligomerization.

Referring to the structure of polymeric L(HBr) shown in Figure 5, it is evident that the dominant gas-phase species obtained during ESI, $[L(HBr_2)]^-$ and $[L(H)]^+$, directly corresponds to the indicated units in the 1D-H-bonded polymer. This correspondence between gas and solution prompted us to revisit the ESI mass spectra in search of larger oligomeric species. Indeed, substantial abundance of the dimeric species $[(L)_2(H_2X)]^+$ and $[(L)_2(H_2X_3)]^-$ were observed (Figures S6 and S7), which can be represented as $[(LH)(Br)(LH)]^+$ and $[(X)(LH)(X)(LH)(X)]^-$ in direct correspondence to the solid-state structure in Figure 5. Although these oligomers were produced by ESI, there is no direct evidence that it is present in the precursor solution, as discussed above. CID of $[(L)_2(H_2Br_3)]^-$ (Figure S9) resulted in elimination of neutral L(HBr) to yield $[L(HBr_2)]^-$. These gas-phase CID results are fully consistent with gas-phase species possessing structures and bonding very closely related to the solid-state data in Figure 5. Finally, ESI of solution of $[L(HBr_2]N^nBu_4$ were similar to the isolated or *in-situ* prepared L(HBr) confirming that this complex is an adequate condensed-phase model for the gas-phase $[L(HBr_2]^-$ adduct (Figure S8).

Condensed Phase Crystallization Process.

In summary, the combination of condensed, gas-phase and *in-silico* methods allows to draw a clear picture of the speciation of the tripodal receptor L when contacted with halides or HX acids. Neutral L has very limited affinity for halides in the gas-phase and therefore no noticeable binding was observed in solution, where intraligand H-bonding interaction are believe to be predominant.[25, 27] Protonation of the central nitrogen disturbs this well-organized network, and in an appropriate solvent (CH_2Cl_2, $CHCl_3$), lead to discrete tripodal anion receptor as crystallized for L(HBr)·2($CHCl_3$) (Figure 4C). However protonation of L to $[L(H)]^+$ creates a situation where the approximate C_3-symmetric tripodal conformer is competed by a "Janus head" form as highlighted by the computational results. This effect is illustrated by multiple lines of evidence, such as the propensity of L(HX) to bind a second halide in solution, the high ESI yield of $[L(HX_2)]^-$, the CID results or the exothermic second halide binding as determined by DFT. From there, aggregation of multiple units can start as corroborated by the observation of $[(L)_2(H_2X_3)]^-$ and $[(L)_2(H_2X)]^+$ by ESI. Moreover, the crystallization of L(HI)·½EtOH is a remarkable example of an arrested aggregation step with both the "tripodal" and "Janus head" forms of $[L(H)]^+$ present (Figure 4B). The processes can then be repeated indefinitely to yield the 1D-H-bonded polymers crystallized for L(HCl) and L(HBr). Overall, the complementary findings between multiple techniques allow us to identify and monitor in detail the key molecular steps underlying the specific precipitation/crystallization of $[L(H)]^+$ (Scheme 4) but may be generalized to a large array of molecules.

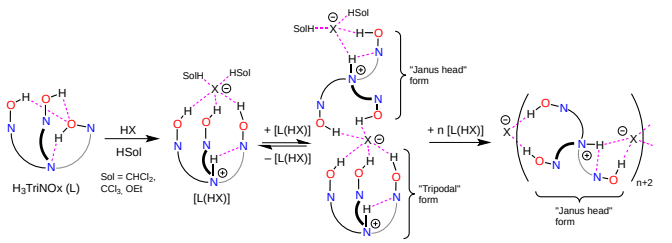

Scheme 4. Schematic oligomerization process for L(HX). H-bonding interactions are depicted in pink.

From Solution to Gas by ESI

Given that ESI resulted in gas-phase complexes that bear compositional correspondence to condensed phase species, we briefly address the nature of ESI vis-à-vis solution speciation. ESI is often considered a "soft" ionization method, largely due to its ability to transfer intact covalently bonded macromolecules from solution to gas, as pioneered by Fenn.[63] However, transferring a charged species from solution to gas necessarily involves drastic changes in the transition from bulk- to micro- to nano- to molecular-"solution" environments, with concomitant opportunities for changes in chemistry, including in speciation.[64] Potential pitfalls in inferring solution speciation from ESI-MS have been emphasized in recent years.[65-68] There are examples of judicious and effective application of ESI-MS to assess condensed phase structures and reactivity of non-covalently bound systems such as supramolecular containers.[69] Highly charged solution metal ions, M^{4+}, were transferred from solution to gas, but only when stabilized against hydrolysis and charge-reduction by multidentate coordinating ligands.[70-72]

Among the dynamic effects during ESI are drastic changes in ion concentrations, including pH.[73] Because solution species that are precursors of the solid 1D-H-bonded coordination polymer are acid adducts of L, L(HX), it is expected that pH changes during ESI, as well halide concentration changes, could affect compositions of gas-phase species. For example, a decrease in pH should generally result in an increase in concentration of the associated weaker acid HI, which could increase the concentration of neutral L(HI) and anionic $[L(HI_2)]^-$. Results such as in Figure 1 may thus reflect aspects of solution speciation, but cannot be taken to directly reveal it. It cannot be concluded from ESI that L is selective for heavier halides in solution, but rather that such selectivity is exhibited in ESI.

CID does demonstrate propensity for particular fragmentation pathways. However, preferred elimination of a particular halide needs to be interpreted in the proper context, such as by comparing energetics for reactions (4) and (6). The overall assessment here is that CID does not necessarily indicate inherently preferential binding of heavier halides, but rather higher stability of lighter hydrogen halides.

Conclusions

Affinity of protonated tripodal hydroxylamine ligand $[L(H)]^+$ for halides X^- was suggested in ESI by abundant gas-phase complexes $[L(HX_2)]^-$. Relative yields from solutions containing more than one halide indicated a preferential affinity for I^- over Br^- over Cl^-. CID of mixed halide complexes $[L(HX_aX_b)]^-$ also revealed preferential retention of the heavier halide in $[L(X_b)]^-$ via elimination of HX_a. Computed DFT energies are in accord with the observed gas-phase speciation and CID fragmentation pathways. Energetics reveal that preferential retention of the heavier halide X_b by $[L(H)]^+$ does not reflect intrinsically higher affinity but rather higher stability of the lighter HX_a product.

Halide affinity of L(HX) was confirmed by binding equilibria constants in solution. The solution results indicated the highest affinity for Cl^-, a lower affinity for Br^-, and the lowest affinity for I^-, which is the opposite of what is observed in gas phase but is in accord with gas-phase affinities obtained after accounting for stabilities of gas-phase HCl, HBr and HI. The 1D polymeric structures of solid L(HX) exhibit a remarkable correspondence to the compositions of gas-phase complexes produced by ESI. The solid structures also bear a close resemblance to computed gas-phase structures. The results suggest hydroxylamines and related substrates as potentially promising for anion reception and recognition.

Conflicts of interest

There are no conflicts to declare.

Acknowledgements

Research at UPenn, Berkeley Lab and Los Alamos was supported as part of the Center for Actinide Science and Technology (CAST), an Energy Frontier Research Center (EFRC) funded by the U.S. Department of Energy (DOE), Office of Science, Basic Energy Sciences (BES), under Award Number DE-SC0016568. Theoretical research was performed using EMSL (grid.436923.9), a DOE Office of Science User Facility sponsored by the Office of Biological and Environmental Research. We acknowledge Prof. Polly L. Arnold (University of Edinburgh) for insightful discussions during the development of this work.

Notes and references

1. Kirk, K. L., *Biochemistry of the Elemental Halogens and Inorganic Halides*. Springer US: 2012.
2. Olander, D. R., The theory of uranium enrichment by the gas centrifuge. *Progress in Nuclear Energy* **1981,** *8* (1), 1-33.
3. Metcalfe, B. L.; Donald, I. W.; Fong, S. K.; Gerrard, L. A.; Strachan, D. M.; Scheele, R. D., Ageing of a phosphate ceramic used to immobilize chloride contaminated actinide waste. *J. Nucl. Mater.* **2009,** *385* (2), 485-488.
4. Fong, S. K.; Donald, I. W.; Metcalfe, B. L., Development of a glass-encapsulated calcium phosphate wasteform for the immobilization of actinide and halide containing radioactive wastes from the pyrochemical reprocessing of plutonium metal. *J. Alloys Compd.* **2007,** *444-445*, 424-428.
5. Riley, B. J.; Vienna, J. D.; Strachan, D. M.; McCloy, J. S.; Jerden, J. L., Materials and processes for the effective capture and immobilization of radioiodine: A review. *J. Nucl. Mater.* **2016,** *470*, 307-326.
6. Ojovan, M. I.; Lee, W. E., *An Introduction to Nuclear Waste Immobilisation*. Elsevier Science: 2013.

7. Hrma, P. R., Retention of Halogen in Waste Glass. U.S. Department of Energy: Pacific Northwest National Laboratory, 2010.
8. Gin, S.; Abdelouas, A.; Criscenti, L. J.; Ebert, W. L.; Ferrand, K.; Geisler, T.; Harrison, M. T.; Inagaki, Y.; Mitsui, S.; Mueller, K. T.; Marra, J. C.; Pantano, C. G.; Pierce, E. M.; Ryan, J. V.; Schofield, J. M.; Steefel, C. I.; Vienna, J. D., An international initiative on long-term behavior of high-level nuclear waste glass. *Mater. Today* **2013,** *16* (6), 243-248.
9. Vienna, J. D., Nuclear Waste Vitrification in the United States: Recent Developments and Future Options. *International Journal of Applied Glass Science* **2010,** *1* (3), 309-321.
10. Peterson, R. A.; Buck, E. C.; Chun, J.; Daniel, R. C.; Herting, D. L.; Ilton, E. S.; Lumetta, G. J.; Clark, S. B., Review of the Scientific Understanding of Radioactive Waste at the U.S. DOE Hanford Site. *Environ. Sci. Technol.* **2018,** *52* (2), 381-396.
11. Noyes, R., *Nuclear Waste Cleanup Technologies and Opportunities*. Elsevier Science: 2013.
12. Billings, A. L.; Fox, K. M., Retention of Sulfate in Savannah River Site High-Level Radioactive Waste Glass. *International Journal of Applied Glass Science* **2010,** *1* (4), 388-400.
13. Park, C. H.; Simmons, H. E., Macrobicyclic amines. III. Encapsulation of halide ions by in,in-1,(k + 2)-diazabicyclo[k.l.m.]alkane ammonium ions. *J. Am. Chem. Soc.* **1968,** *90* (9), 2431-2432.
14. Graf, E.; Lehn, J. M., Anion cryptates: highly stable and selective macrotricyclic anion inclusion complexes. *J. Am. Chem. Soc.* **1976,** *98* (20), 6403-6405.
15. Sessler, J. L.; Gale, P.; Cho, W. S., *Anion Receptor Chemistry*. Royal Society of Chemistry: 2007.
16. He, Q.; Tu, P.; Sessler, J. L., Supramolecular Chemistry of Anionic Dimers, Trimers, Tetramers, and Clusters. *Chem* **2018,** *4* (1), 46-93.
17. Ayme, J.-F.; Beves, J. E.; Campbell, C. J.; Gil-Ramírez, G.; Leigh, D. A.; Stephens, A. J., Strong and Selective Anion Binding within the Central Cavity of Molecular Knots and Links. *J. Am. Chem. Soc.* **2015,** *137* (31), 9812-9815.
18. Liu, Y.; Sengupta, A.; Raghavachari, K.; Flood, A. H., Anion Binding in Solution: Beyond the Electrostatic Regime. *Chem* **2017,** *3* (3), 411-427.
19. Busschaert, N.; Caltagirone, C.; Van Rossom, W.; Gale, P. A., Applications of Supramolecular Anion Recognition. *Chem. Rev.* **2015,** *115* (15), 8038-8155.
20. Langton, M. J.; Serpell, C. J.; Beer, P. D., Anion Recognition in Water: Recent Advances from a Supramolecular and Macromolecular Perspective. *Angew. Chem. Int. Ed.* **2016,** *55* (6), 1974-1987.
21. Ahmed, L.; Rhaman, M. M.; Mendy, J. S.; Wang, J.; Fronczek, F. R.; Powell, D. R.; Leszczynski, J.; Hossain, M. A., Experimental and Theoretical Studies on Halide Binding with a p-Xylyl-Based Azamacrocycle. *J. Phys. Chem. A* **2015,** *119* (2), 383-394.
22. Gale, Philip A.; Howe, Ethan N. W.; Wu, X., Anion Receptor Chemistry. *Chem* **2016,** *1* (3), 351-422.
23. Liu, Y.; Zhao, W.; Chen, C.-H.; Flood, A. H., Chloride capture using a C–H hydrogen bonding cage. *Science* **2019**, eaaw5145.
24. Brown, A.; Beer, P. D., Halogen bonding anion recognition. *Chem. Commun.* **2016,** *52* (56), 8645-8658.
25. Bogart, J. A.; Lippincott, C. A.; Carroll, P. J.; Schelter, E. J., An Operationally Simple Method for Separating the Rare-Earth Elements Neodymium and Dysprosium. *Angewandte Chemie International Edition* **2015,** *54* (28), 8222-8225.
26. Fang, H.; Cole, B. E.; Qiao, Y.; Bogart, J. A.; Cheisson, T.; Manor, B. C.; Carroll, P. J.; Schelter, E. J., Electro-kinetic Separation of Rare Earth Elements Using a Redox-Active Ligand. *Angew. Chem. Int. Ed.* **2017,** *56* (43), 13450-13454.
27. Cole, B. E.; Falcones, I. B.; Cheisson, T.; Manor, B.; Carroll, P.; Schelter, E. J., A Molecular Basis to Rare Earth Separations for Recycling: Tuning TriNOx Ligand Properties for Improved Performance. *Chem. Commun.* **2018,** *54*, 10276–10279.
28. Cheisson, T.; Solola, L. A.; Gau, M. R.; Carroll, P. J.; Schelter, E. J., Silyl Transfer Pathway to a Ce(IV) Imido Complex. *Organometallics* **2018,** *37* (23), 4332-4335.
29. McSkimming, A.; Su, J.; Cheisson, T.; Gau, M. R.; Carroll, P. J.; Batista, E. R.; Yang, P.; Schelter, E. J., Coordination Chemistry of a Strongly-Donating Hydroxylamine with Early Actinides: An Investigation of Redox Properties and Electronic Structure. *Inorg. Chem.* **2018,** *57* (8), 4387-4394.
30. Cheisson, T.; Cole, B. E.; Manor, B. C.; Carroll, P. J.; Schelter, E. J., Phosphoryl-Ligand Adducts of Rare Earth-TriNOx Complexes: Systematic Studies and Implications for Separations Chemistry. *ACS Sustainable Chem. Eng.* **2019,** *7* (5), 4993-5001.
31. Cole, B. E.; Cheisson, T.; Higgins, R. F.; Nakamaru-Ogiso, E.; Manor, B. C.; Carroll, P. J.; Schelter, E. J., Redox-Driven Chelation and Kinetic Separation of Select Rare Earths Using a Tripodal Nitroxide Proligand. *Inorg. Chem.* **2019**.
32. Shannon, R., Revised effective ionic radii and systematic studies of interatomic distances in halides and chalcogenides. *Acta Crystallogr. Sect. A* **1976,** *32* (5), 751-767.
33. Rahm, M.; Zeng, T.; Hoffmann, R., Electronegativity Seen as the Ground-State Average Valence Electron Binding Energy. *J. Am. Chem. Soc.* **2019,** *141* (1), 342-351.
34. Eller, K.; Schwarz, H., Organometallic Chemistry in the Gas-Phase. *Chem. Rev.* **1991,** *91* (6), 1121-1177.
35. Schalley, C. A.; Hornung, G.; Schroder, D.; Schwarz, H., Mass spectrometric approaches to the reactivity of transient neutrals. *Chem. Soc. Rev.* **1998,** *27* (2), 91-104.
36. Meot-Ner, M., Update 1 of: Strong Ionic Hydrogen Bonds. *Chem. Rev.* **2012,** *112* (10), PR22-PR103.
37. O'Hair, R. A. J., The 3D quadrupole ion trap mass spectrometer as a complete chemical laboratory for fundamental gas-phase studies of metal mediated chemistry. *Chem. Commun.* **2006,** (14), 1469-1481.
38. Legon, A. C., The Nature of Ammonium and Methylammonium Halides in the Vapor-Phase - Hydrogen-Bonding Versus Proton-Transfer. *Chem. Soc. Rev.* **1993,** *22* (3), 153-163.
39. Walker, B. W.; Sunderlin, L. S., The thermochemistry of formic acid halide anion clusters. *Int. J. Mass spectrom.* **1999,** *184* (2-3), 183-189.
40. Bogdanov, B.; McMahon, T. B., An ab initio and density functional theory investigation of the structures and energetics of halide ion-alcohol complexes in the gas phase. *J. Phys. Chem. A* **2000,** *104* (33), 7871-7880.
41. Hiraoka, K.; Katsuragawa, J.; Sugiyama, T.; Kojima, T.; Yamabe, S., Hydrogen bonds in gas-phase clusters between halide ions and olefins. *J. Am. Soc. Mass. Spectrom.* **2001,** *12* (2), 144-149.
42. Gillis, E. A. L.; Demireva, M.; Sarwar, M. G.; Chudzinski, M. G.; Taylor, M. S.; Williams, E. R.; Fridgen, T. D., Structure and energetics of gas phase halogen-bonding in mono-, bi-, and tri-dentate anion receptors as studied by BIRD. *Phys. Chem. Chem. Phys.* **2013,** *15* (20), 7638-7647.
43. Chiavarino, B.; Crestoni, M. E.; Maitre, P.; Fornarini, S., Halide adducts of 1,3,5-trinitrobenzene: Vibrational signatures and role of anion-pi interactions. *Int. J. Mass spectrom.* **2013,** *354*, 62-69.
44. O'Brien, J. T.; Prell, J. S.; Berden, G.; Oomens, J.; Williams, E. R., Effects of anions on the zwitterion stability of Glu, His and Arg

investigated by IRMPD spectroscopy and theory. *Int. J. Mass spectrom.* **2010,** *297* (1-3), 116-123.
45. Corinti, D.; Gregori, B.; Guidoni, L.; Scuderi, D.; McMahon, T. B.; Chiavarino, B.; Fornarini, S.; Crestoni, M. E., Complexation of halide ions to tyrosine: role of non-covalent interactions evidenced by IRMPD spectroscopy. *Phys. Chem. Chem. Phys.* **2018,** *20* (6), 4429-4441.
46. Cheisson, T.; Schelter, E. J., Rare Earths Elements: Mendeleev's Bane, Modern Marvels. *Science* **2019,** *363*, 489–493.
47. Rutkowski, P. X.; Michelini, M. C.; Gibson, J. K., Gas-phase lanthanide chloride clusters: relationships among ESI abundances and DFT structures and energetics. *Phys. Chem. Chem. Phys.* **2012,** *14* (6), 1965-1977.
48. Dau, P. D.; Gibson, J. K., Halide Abstraction from Halogenated Acetate Ligands by Actinyls: A Competition between Bond Breaking and Bond Making. *J. Phys. Chem. A* **2015,** *119* (13), 3218-3224.
49. Lias, S. G.; Bartmess, J. E.; Liebman, J. F.; Holmes, J. L.; Levin, R. D.; Mallard, W. G., Gas-Phase Ion and Neutral Thermochemistry. *J. Phys. Chem. Ref. Data* **1988,** *17* (1), 1-861.
50. Blanksby, S. J.; Ellison, G. B., Bond Dissociation Energies of Organic Molecules. *Acc. Chem. Res.* **2003,** *36* (4), 255-263.
51. Cooks, R. G.; Wong, P. S. H., Kinetic method of making thermochemical determinations: Advances and applications. *Accounts of Chemical Research* **1998,** *31* (7), 379-386.
52. Ellis, R. J.; Chartres, J.; Henderson, D. K.; Cabot, R.; Richardson, P. R.; White, F. J.; Schröder, M.; Turkington, J. R.; Tasker, P. A.; Sole, K. C., Design and Function of Pre-organised Outer-Sphere Amidopyridyl Extractants for Zinc(II) and Cobalt(II) Chlorometallates: The Role of C–H Hydrogen Bonds. *Chem. Eur. J.* **2012,** *18* (25), 7715-7728.
53. Turkington, J. R.; Bailey, P. J.; Love, J. B.; Wilson, A. M.; Tasker, P. A., Exploiting outer-sphere interactions to enhance metal recovery by solvent extraction. *Chem. Commun.* **2013,** *49* (19), 1891-1899.
54. Carson, I.; MacRuary, K. J.; Doidge, E. D.; Ellis, R. J.; Grant, R. A.; Gordon, R. J.; Love, J. B.; Morrison, C. A.; Nichol, G. S.; Tasker, P. A.; Wilson, A. M., Anion Receptor Design: Exploiting Outer-Sphere Coordination Chemistry To Obtain High Selectivity for Chloridometalates over Chloride. *Inorg. Chem.* **2015,** *54* (17), 8685-8692.
55. Al-Shnani, F.; Guisado-Barrios, G.; Sainz, D.; Peris, E., Tris-triazolium Salts as Anion Receptors and as Precursors for the Preparation of Cylinder-like Coordination Cages. *Organometallics* **2019,** *38* (3), 697-701.
56. Sengupta, A.; Liu, Y.; Flood, A. H.; Raghavachari, K., Anion-Binding Macrocycles Operate Beyond the Electrostatic Regime: Interaction Distances Matter. *Chem. Eur. J.* **2018,** *24* (54), 14409-14417.
57. Nepal, B.; Scheiner, S., Competitive Halide Binding by Halogen Versus Hydrogen Bonding: Bis-triazole Pyridinium. *Chem. Eur. J.* **2015,** *21* (38), 13330-13335.
58. Lee, S. J. R.; Mullinax, J. W.; Schaefer, H. F., Intermolecular interactions and proton transfer in the hydrogen halide–superoxide anion complexes. *Phys. Chem. Chem. Phys.* **2016,** *18* (8), 6201-6208.
59. Pramanik, A.; Powell, D. R.; Wong, B. M.; Hossain, M. A., Spectroscopic, Structural, and Theoretical Studies of Halide Complexes with a Urea-Based Tripodal Receptor. *Inorg. Chem.* **2012,** *51* (7), 4274-4284.
60. Ulatowski, F.; Dąbrowa, K.; Bałakier, T.; Jurczak, J., Recognizing the Limited Applicability of Job Plots in Studying Host–Guest Interactions in Supramolecular Chemistry. *J. Org. Chem.* **2016,** *81* (5), 1746-1756.
61. Thordarson, P., Determining association constants from titration experiments in supramolecular chemistry. *Chem. Soc. Rev.* **2011,** *40* (3), 1305-1323.
62. de Namor, A. F. D.; Shehab, M., Selective recognition of halide anions by calix[4]pyrrole: A detailed thermodynamic study. *J. Phys. Chem. B* **2003,** *107* (26), 6462-6468.
63. Whitehouse, C. M.; Dreyer, R. N.; Yamashita, M.; Fenn, J. B., Electrospray Interface for Liquid Chromatographs and Mass Spectrometers. *Anal. Chem.* **1985,** *57* (3), 675-679.
64. Kebarle, P.; Verkerk, U. H., Electrospray: From Ions in Solution to Ions in the Gas Phase, What We Know Now. *Mass Spectrom. Rev.* **2009,** *28* (6), 898-917.
65. Di Marco, V. B.; Bombi, G. G.; Zambon, S.; Traidi, P., Metal-ligand solution equilibria studied by electrospray ionization mass spectrometry: effect of instrumental parameters. *J. Mass Spectrom.* **2009,** *44* (1), 120-127.
66. Di Marco, V. B.; Raveane, L.; Dean, A.; Traldi, P., Perturbations produced by electrospray ionization mass spectrometry in the speciation of aluminium(III)/1,6-dimethy1-4-hydroxy-3-pyridinecarboxylate aqueous solutions. *Rapid Commun. Mass Spectrom.* **2010,** *24* (7), 868-874.
67. McDonald, L. W.; Campbell, J. A.; Clark, S. B., Failure of ESI Spectra to Represent Metal-Complex Solution Composition: A Study of Lanthanide-Carboxylate Complexes. *Anal. Chem.* **2014,** *86* (2), 1023-1029.
68. Swadzba-Kwasny, M., Comment on "Lewis acidic ionic liquids of crown ether complex cations: preparation and applications in organic reactions" by Y. Liang, J. Wang, C. Cheng and H. Jing, RSC Adv., 2016, 6, 93546. *RSC Adv.* **2017,** *7* (82), 51907-51909.
69. Qi, Z. H.; Heinrich, T.; Moorthy, S.; Schalley, C. A., Gas-phase chemistry of molecular containers. *Chem. Soc. Rev.* **2015,** *44* (2), 515-531.
70. Gong, Y.; Hu, H. S.; Tian, G. X.; Rao, L. F.; Li, J.; Gibson, J. K., A Tetrapositive Metal Ion in the Gas Phase: Thorium(IV) Coordinated by Neutral Tridentate Ligands. *Angew Chem Int Edit* **2013,** *52* (27), 6885-6888.
71. Gong, Y.; Tian, G. X.; Rao, L. F.; Gibson, J. K., Tetrapositive Plutonium, Neptunium, Uranium, and Thorium Coordination Complexes: Chemistry Revealed by Electron Transfer and Collision Induced Dissociation. *J. Phys. Chem. A* **2014,** *118* (15), 2749-2755.
72. Rutkowski, P. X.; Michelini, M. D.; Gibson, J. K., Proton Transfer in Th(IV) Hydrate Clusters: A Link to Hydrolysis of Th(OH)(2)(2+) to Th(OH)(3)(+) in Aqueous Solution. *J. Phys. Chem. A* **2013,** *117* (2), 451-459.
73. Konermann, L., Addressing a Common Misconception: Ammonium Acetate as Neutral pH "Buffer" for Native Electrospray Mass Spectrometry. *J. Am. Soc. Mass. Spectrom.* **2017,** *28* (9), 1827-1835.

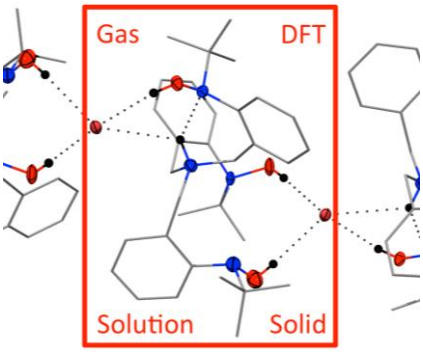

The binding of halide anions with a tripodal hydroxylamine ligand studied in gas (mass spectrometry and DFT methods) and condensed phases revealed notable agreement.